

## RELAXATION IN $N$ -BODY SIMULATIONS OF SPHERICAL SYSTEMS

J. A. SELLWOOD

Department of Physics and Astronomy, Rutgers University,  
136 Frelinghuysen Road, Piscataway, NJ 08854  
sellwood@physics.rutgers.edu

*Draft on June 10, 2019*

### ABSTRACT

I present empirical measurements of the rate of relaxation in  $N$ -body simulations of stable spherical systems and distinguish two separate causes of relaxation: two-body effects, which cause energy exchange between particles of differing masses, and collective oscillations driven by shot noise that lead to an enhanced energy diffusion rate. I use four different methods to compute the gravitational field, and a 100-fold range in the numbers of particles in each case. I find the rate at which energy is exchanged between particles of differing masses does not depend at all on the force determination method, but I do find the energy diffusion rate, which is substantially enhanced by collective modes, is marginally lower when a field method is used. The relaxation rate in 3D is virtually independent of the method used because it is dominated by distant encounters; any method to estimate the gravitational field that correctly captures the contributions from distant particles must also capture their statistical fluctuations and the collective modes they drive.

*Subject headings:* Galaxies: kinematics and dynamics — numerical methods

### 1. INTRODUCTION

A rough estimate of the ratio of the relaxation time to the crossing time in a gravitating system of  $N$  equal mass particles is  $t_{\text{relax}}/t_{\text{cross}} \sim 0.1N/\ln N$  (*e.g.* Binney & Tremaine 2008). While this formula is very approximate, a more careful derivation is not warranted since  $t_{\text{relax}} \sim 1000t_{\text{cross}}$  when  $N = 10^5$  only, implying that an  $N$ -body simulation with this few particles should manifest collisionless behavior for a reasonable period of evolution; furthermore, modern simulations generally use much larger numbers of particles. It should be noted that this formula applies for pressure-supported systems, not disks (Sellwood 2013), is nominally for point mass particles, and also neglects collective effects.

Numerical methods used to compute the gravitational field in simulations that aspire to be collisionless fall into three broad categories. The most popular direct method is some type of tree code (*e.g.* Barnes & Hut 1986; Springel 2005) that effectively sums the attraction of every particle pair, with a softening kernel to limit the magnitude of the acceleration at short range. The far more efficient (Sellwood 2014) particle-mesh methods (PM, *e.g.* Hockney & Eastwood 1981) determine the gravitational field on a raster of points that has some appropriate geometry; forces at the actual particle positions are computed by interpolation between grid points. Finally, the least popular are field methods (*e.g.* Clutton-Brock 1972; Hernquist & Ostriker 1992) that expand the density and potential in a basis set of functions that should be chosen such that truncating the expansion at low order yields an adequate approximation to the field.

It is often argued (*e.g.* Weinberg & Katz 2007a,b) that the various  $N$ -body methods differ widely in their ability to hide the lumpiness of the potential from a set of point masses and that field methods, in particular, have “relaxation times ... orders of magnitude longer” than in tree codes. This claim was based on a lengthy calculation using Hamiltonian mechanics, but a more heuristic argument is the number of terms needed to define the potential: a well-

chosen basis may yield an adequate approximation to the total field from a small number of terms. The shot noise in each term varies as  $N^{-1/2}$ , since all particles contribute, but only the lowest order monopole term has a large value about which shot noise fluctuations are small. However, the amplitudes of the aspherical terms, which are oscillatory, depend on the almost-complete cancellation of the  $N$  contributions, and are entirely noise-driven in a spherical model, for example.

The number of values that define the potential in PM codes is  $n_{\text{grid}}$  and, since each mesh point typically hosts  $\sim N/n_{\text{grid}}$  particles, each separate value will be subject to a greater degree of shot noise. In direct methods, there are  $N$  separate contributions to the field. This argument also overstates the case since the potential is the double integral of the density; in effect, the potential kernel, which is monotonic and has infinite range, implies the field at each point is the sum of contributions from all the sources, and potential variations are therefore far smoother than could be supported by an arbitrary function defined by the same number of values.

Hernquist & Barnes (1990, hereafter HB90) used a King model for an experimental comparison between the relaxation rates in simulations when the gravitational field was determined by three different methods, and Hernquist & Ostriker (1992) extended their results to include a field method. They found that the rate of energy diffusion of particles was only mildly affected by the method used. While their evidence was quite strong, they generally employed only 4096 particles and gravity softening spoiled the equilibrium of some of their initial models.

Here I present a further study that uses two distinct measures of the “relaxation” rate. The energy diffusion rate reported by HB90, and a measure of the rate of energy exchange between particle species of differing masses. The former measure includes all sources of relaxation, especially collective effects, while the latter is a more direct measure of the 2-body collision rate.

## 2. MODELS

In order to illustrate the importance of collective effects, I here report measurements in three different mass models. All three are spheres with ergodic (isotropic) distribution functions (DFs) that are therefore stable equilibria.

The mass models are:

- a **Hernquist model** Hernquist (1990) developed a simple spherical model having the centrally cusped density profile

$$\rho(r) = \frac{Ma}{2\pi r(r+a)^3}, \quad (1)$$

which has the potential  $\Phi(r) = -GM/(a+r)$ . Here  $a$  is a length scale and  $M$  the finite total mass integrated to infinity. Hernquist also gave the equilibrium isotropic distribution function for this density and potential. I truncate this model so that no particle has sufficient energy to stray beyond  $r = 10a$ , which causes the density profile to taper smoothly to zero at that radius, and discards  $\sim 26\%$  of the mass, but leaves the density profile as given by eq. (1) over the range  $0 \leq r/a \lesssim 5$ .

- b **Plummer sphere** Plummer (1911) introduced one of the most widely used spherical mass models in astronomy. It has the cored density profile

$$\rho(r) = \frac{3M}{4\pi a^3} (1+x^2)^{-5/2}, \quad (2)$$

where  $x = r/a$  and  $M$  is the total mass. The potential is  $\Phi(r) = -(GM/a)(1+x^2)^{-1/2}$ , and the isotropic DF is that of a polytrope of index 5 (see BT08). Applying an energy truncation so that no particle passes outside  $r = 10a$  discards only  $\sim 3.4\%$  of the mass in this model with its lower density envelope.

- c **Uniform sphere** with density  $\rho_0 = 3M/(4\pi a^3)$ , where  $a$  is the outer radius. Polyachenko & Shukhman (1979) give the isotropic DF for a homogeneous sphere with a sharp outer boundary. The harmonic potential in the interior of this unusual model implies that all particles have the same orbital frequencies; this model, therefore, affords a dramatic illustration of the role of collective effects.

In all cases, I employ two equally numerous sets of particles drawn from the DF: the masses of particles,  $m_i = \mu_i m_*$  are such that those of one sample have  $\mu_i = 9$  and the other have  $\mu_i = 1$ , and  $m_*$  is chosen such that the combined density profile is that given by the above expressions. Debattista & Sellwood (2000, appendix A) describe an optimal method of drawing particle coordinates from a DF in such a way as to reduce shot noise in the distribution of energies. Sellwood (2014) reports results that show the material benefit of this strategy.

The models are evolved for 100 dynamical times, where  $t_0 = (a^3/GM)^{1/2}$ , with a timestep of  $0.02t_0$  for the uniform sphere and Plummer models. The basic step for the Hernquist model is 0.0125 but time steps are increased, in this case only, by four successive factors of 2 at appropriate radii. I save the instantaneous energy of a representative set of particles ( $2 \times 10^4$  or all, whichever is the less) after every dynamical time.

## 3. METHODS

I employ four different numerical methods to determine the gravitational field from the particles:

1. **BHT** A tree code that uses the scheme first proposed by Barnes & Hut (1986). I include dipole terms and particle groupings are opened when they subtend an angle  $> \theta_{\max} = 0.5$  radians. Forces are softened at short range only using the kernel advocated by Monaghan (1992), with  $\epsilon = 0.05a$  for the uniform sphere and  $\epsilon = 0.1a$  for the other two models.
2. **S3D** A spherical grid, which is a hybrid PM expansion method that expands the non-spherically symmetric part in surface harmonics on a set of spherical shells (McGlynn 1984; Sellwood 2003). Force discontinuities, which arise when particle radii cross, are eliminated by adopting linear interpolation between radial shells. I tabulate the expansion coefficients at 100 logarithmically spaced radii, and expand in azimuth up to  $l_{\max} = 8$ .
3. **SFP** A field method that employs a biorthonormal set of basis functions (Clutton-Brock 1972; Hernquist & Ostriker 1992), which I name SFP (for smooth field-particle) but is also known as SCF. I expand in azimuth up to  $l_{\max} = 8$  and employ radial functions up to  $n_{\max} = 10$ . I use this method for the Plummer and Hernquist models only.
4. **C3D** I do not use the SFP method for the uniform sphere, but employ a PM method that uses 3D Cartesian grid (James 1977), and I set  $a = 50$  mesh spaces. The grid has  $129^3$  points, except for the lowest  $N$  case where it was  $257^3$  points in order to allow plenty of room for expansion of the particle distribution. Linear interpolation results in the inter-particle force given in Sellwood & Merritt (1994, appendix), which is well approximated by cubic density kernel with  $\epsilon \approx 1.8$  grid spaces (Sellwood 2014).

More details of all these methods are given in the on-line manual (Sellwood 2014).

The tree code uses explicit particle softening, while short-range forces are implicitly smoothed in the Cartesian grid. These methods therefore do not yield the exact Newtonian potential of the mass distribution. In order to ensure that the initial model is in equilibrium in the tree code, I use the largest  $N$  simulation of each type to tabulate the difference between the spherically averaged central attraction of the particles at  $t = 0$  and the analytic central attraction at a 1D array of points; I then interpolate from this table a supplementary central attraction that is added to the tree-determined force on each particle before its motion is advanced. I use a similar procedure for the 3D Cartesian grid, but in order to avoid shot noise in the (very small) permanent part of central attraction, the numerical force is computed from a smooth density distribution assigned to the grid. These generally small corrections are not needed for S3D or SFP methods.

With these fixed correction terms in C3D and BHT, and with a coordinate center for the S3D and SFP methods, it

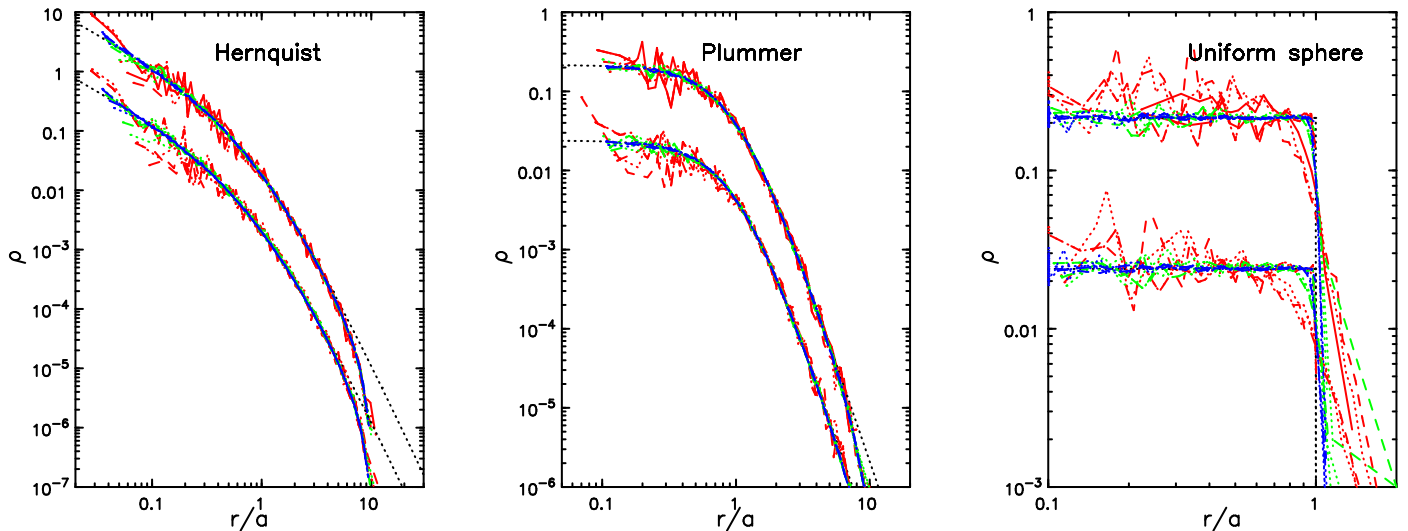


FIG. 1.— The final density profiles measured from the separate mass particles, which contribute 10% and 90% of the total density, in all 27 simulations. In each panel, the color indicates the number of particles: red is for  $N = 4 \times 10^3$ , green is for  $N = 4 \times 10^4$  and blue is for  $N = 4 \times 10^5$ . The different methods for computing the field are distinguished by the line styles: solid is for S3D, dotted is for BHT, and dashed is for either SFP (Hernquist and Plummer) or C3D (uniform sphere). The black dotted curves indicate the expected density profile of each mass species; no particles in the left and middle panels started with enough energy to pass beyond  $r = 10a$ .

is important to ensure that the initial set of particles is at rest and centered in this coordinate frame. After creating the initial set of particles, I therefore adjust the positions and speeds by a small amount to ensure the center of mass is at the coordinate center and the model has no net momentum. An alternative strategy that would achieve the same outcome would be to shift the grid (or expansion) center at frequent intervals. I also experimented with inserting mirror pairs of particles having coordinates  $(\mathbf{x}, \mathbf{v})$  and  $(-\mathbf{x}, -\mathbf{v})$ , in a step towards a quiet start, but this strategy had the undesirable (for this study) effects of eliminating any lop-sided, and emphasizing the bi-symmetric, contributions to the total field.

The instantaneous energy of the  $i$ th particle is approximately

$$\mathcal{E}_i = m_i E_i(t) = m_i \left[ \Phi(\mathbf{x}_i) + \frac{1}{2} v_i^2 \right], \quad (3)$$

where  $E_i$  is the specific energy of the particle, or energy per unit mass,  $\Phi$  is the estimated gravitational potential at the particle position,  $\mathbf{x}_i(t)$ , and  $v_i(t)$  is the scalar speed of the particle. This definition is exact only for a particle of infinitesimal mass, since a finite mass particle contributes to  $\Phi$ . The energy required to disperse a system of gravitating particles, the total energy, is  $\mathcal{E}_{\text{tot}} = T + W$ , where  $T = \sum_i \frac{1}{2} m_i v_i^2$  and  $W = \frac{1}{2} \sum_i m_i \Phi(\mathbf{x}_i)$ , and the  $W$  term is halved because the summation over the  $\Phi$  values includes every pair of particles twice. The total energy, defined this way is very well conserved in the simulations, whereas the sum of the energies (eq. 3),  $\sum_i \mathcal{E}_i = T + 2W$ , is clearly *not* the total energy, and is not conserved.

In order to test for virial equilibrium of an  $N$ -body simulation, it is better to measure the virial of Clausius,  $W_c \equiv \sum_i m_i \mathbf{x}_i \cdot \mathbf{a}_i$ , since the inter-particle forces are not perfectly Newtonian, especially at short range. It is easy to show that  $W_c = W$  for precisely inverse-square law accelerations. The particle distribution is in equilibrium when  $2T = |W_c|$ .

It is convenient to choose units such that  $G = M = a = 1$ , so that the dynamical time  $t_0 = (a^3/GM)^{1/2} = 1$ , for example. A convenient scaling to physical units for the inhomogeneous models is to choose  $a = 3$  kpc and  $t_0 = 10$  Myr, which implies  $M = 6 \times 10^{10} M_\odot$  and velocities scale as  $(GM/a)^{1/2} \simeq 293$  km/s.

#### 4. RESULTS

Figure 1 shows the final ( $t = 100t_0$ ) density profiles in all 27 simulations. The three panels show the different mass models. Within each panel the curves drawn in red are from the lowest  $N = 4 \times 10^3$ , those in green employ  $4 \times 10^4$  particles, and those in blue  $4 \times 10^5$ , with  $N/2$  in each mass species so that the initial densities from each species differ by factors of nine, as shown. The field is determined on the S3D grid for the full-drawn curves, the BHT method for the dotted curves, while the dashed curves are from either the SFP, for the Hernquist and Plummer models, or C3D for the uniform sphere.

The density profiles of the models evolve insignificantly for the largest  $N$  (blue curves), confirming that the models are stable equilibria. As expected, relaxation drives the greatest changes in the simulations with the smallest  $N$  (red curves) where, in a few cases, there are hints of some slight segregation of the particles of different masses over the time interval computed.

##### 4.1. Collective modes

Figure 2 shows the time evolution of the virial ratio,  $T/|W_c|$  in all 27 simulations reported here. The three panels show the different mass models and the colors and line styles are used to distinguish the particle number and field determination method, as in Fig. 1.

It is clear from Figure 2 that the virial ratio  $T/|W_c|$  remains close to  $\frac{1}{2}$  for the duration of all these simulations, and the fluctuations around this ratio are largest for the

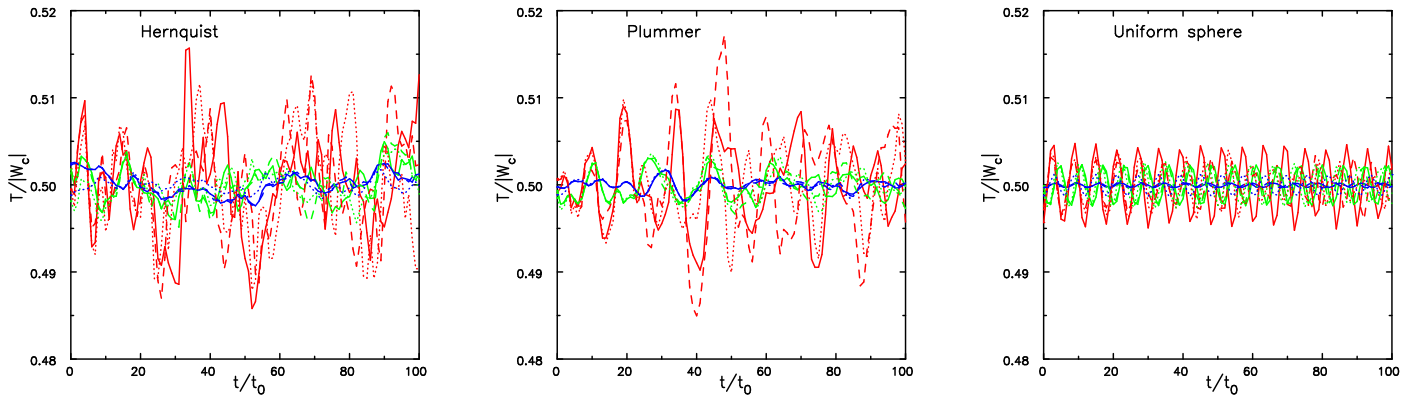


FIG. 2.— The time evolution of the virial ratio in all 27 simulations. As for Fig. 1, the color indicates the number of particles while the different methods for computing the field are distinguished by the line styles.

lowest  $N$  (red curves) and smallest for the highest  $N$  (blue curves). The fluctuations are aperiodic for the inhomogeneous models, but are periodic in the uniform sphere, where they have very nearly the same period,  $2\pi t_0$ , in all nine simulations. Furthermore, the initial behavior of the curves for models with the same  $N$  (color) is very similar for the different field determination methods, because the models were set-up using particles having the same positions and velocities. The red curves diverge quite noticeably, but the blue curves for the SCF and S3D methods remain barely distinguishable to the end; a slightly different value of  $W_c$  arises in the BHT code because the forces differ due to softening and corrective terms, which is the reason the dotted curves remain distinct, particularly in the Hernquist model.

These fluctuations are driven by collective modes that are excited by shot-noise in the finite number of particles, as was recognized long ago by Rostoker & Rosenbluth (1960) in the context of collisionless plasmas, and has been studied in gravitating systems by Weinberg (1998) and others. The amplitudes of the modes should scale as  $N^{-1/2}$ , which is the reason the fluctuations in  $T/|W_c|$  decrease with increasing  $N$ . The modes have essentially the same frequency in the uniform sphere where they appear to be almost undamped. Modes in collisionless systems can be damped only through resonant exchanges between the mode and the particles, and conditions for resonant damping are highly unfavorable because all particles have the same frequencies in this harmonic potential.

The aperiodic fluctuations in the inhomogeneous models (left and middle panels) reflect the broader range of frequencies among the particles in these models. Collective oscillations that are excited by shot noise in these cases are almost certainly quickly damped at resonances, yet the amplitudes fluctuate greatly with neither a clear decaying, nor a growing, trend.

#### 4.2. Energy diffusion and exchange

Figure 3 presents a typical set of energy measurements from the particles in a simulation; values for heavy particles are drawn in red, while green is used for the light particles. The left panel gives the value of  $\langle [E_i(0) - E_i(t)]^2 \rangle$ , the mean square change since the start in the measured spe-

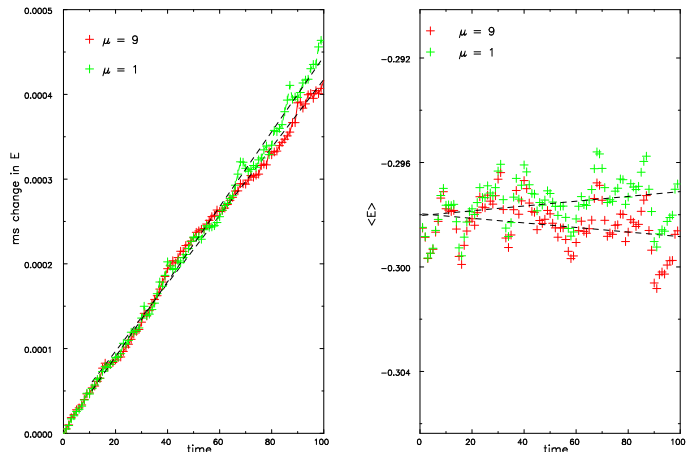


FIG. 3.— Results from a run of a Hernquist model with  $N = 2 \times 10^4$  particles of each mass when forces are determined using the field method (SFP). The left panel shows the mean square change of energy of the particles, while the right panel shows the evolution of the mean specific energy (per unit mass) of the particles of each mass species.

cific energy of the particles. It can be seen that the value of this quantity rises roughly linearly with time, as HB90 found, indicating that the values are changing through a diffusive process. I fit a straight line to the last 90 values (*i.e.* ignoring the first 11, where the rise is often a little steeper), and henceforth report only this fitted slope as the mean square change of  $E$  per dynamical time  $t_0$ , and its associated uncertainty.

The right panel of Figure 3 gives the time evolution of the mean specific energy  $\langle E_i(t) \rangle$  of the particles of the separate masses.<sup>1</sup> The rapid variations have the same sign for each particle species because they arise from variations in  $T + 2W$  that are related to the virial fluctuations (Fig. 2). They result from evolving density changes seeded by shot-noise driven fluctuations among the particles.

<sup>1</sup> The mean energy measured from the simulation,  $\langle E_i(0) \rangle \approx -0.30$ , is somewhat higher than that expected from the distribution function,  $\langle E \rangle \approx -0.356$ , because the potential well in the simulation determined from the selected particles, which are only 74% of the total mass, is not as deep as the analytic potential of the untruncated model.

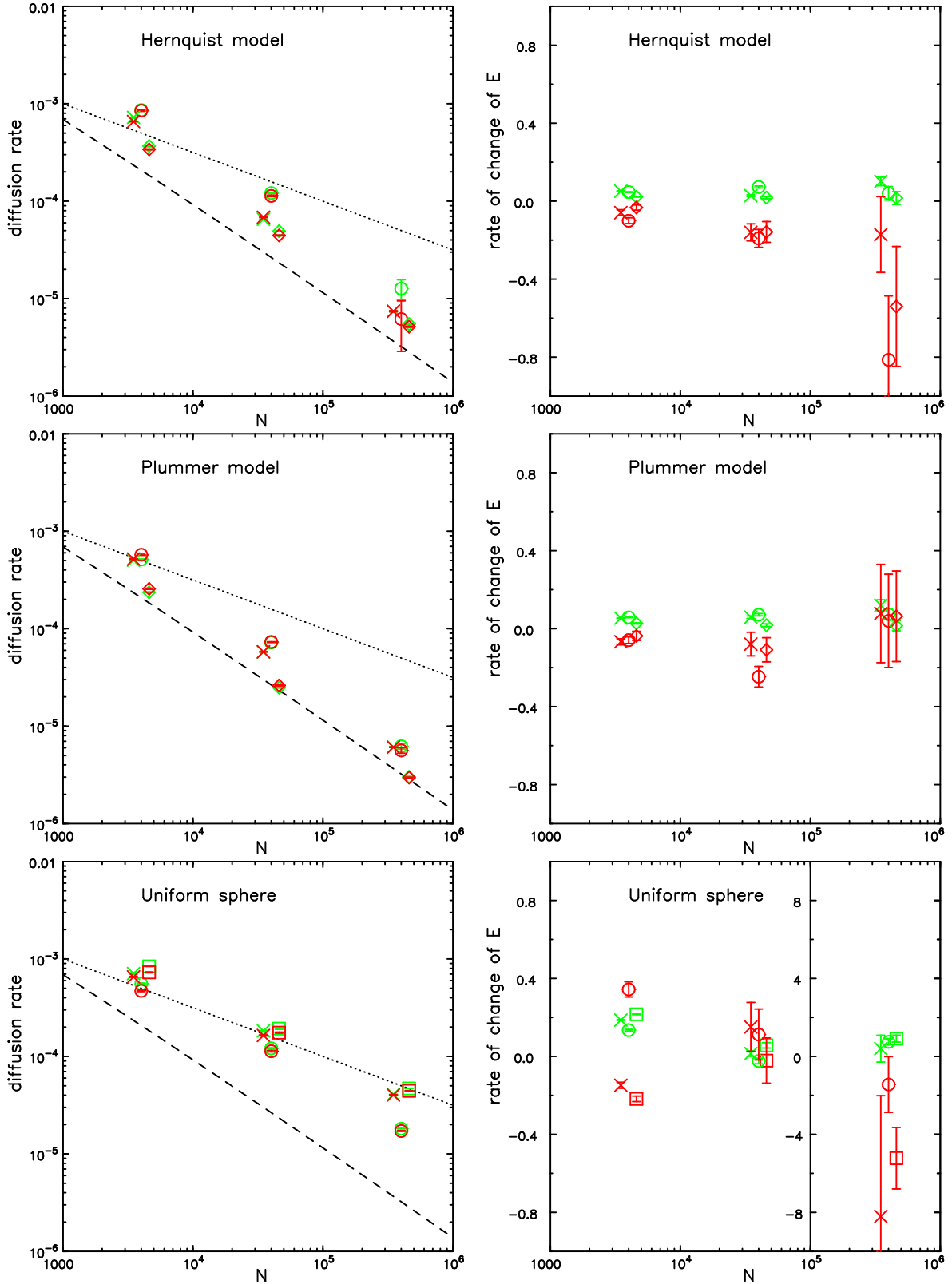


FIG. 4.— Summary of results from 27 simulations. The left column shows the  $N$ -dependence of the diffusion rate defined in eq. (4) and the right column shows  $Nd\langle E_i(t) \rangle/dt$ , with green points for the light particles and red for the nine times heavier particles. The top row is for the Hernquist model, the middle row for the Plummer model and the bottom row is for the uniform sphere. Crosses are from the tree code (BHT), circles from the spherical grid (S3D), diamonds from the field method (SFP) which was used for the Hernquist and Plummer models only, while squares are for a cubic Cartesian grid (C3D) which was used for the uniform sphere only. The error bars show  $\pm\sigma$  uncertainties in the slopes, and the symbols from the different methods have been slightly shifted horizontally for clarity even though the same total numbers of particles,  $N$ , were used. Note that the vertical scale is expanded by a factor of 10 for the points at the highest  $N$  in the lower right panel.

In addition to these fluctuations, the right panel of Figure 3 displays a gradual divergence of the mean energies of the heavy and light particles, which represents the gradual exchange of energy that would in the long-run cause the heavy particles to settle to the center and the lighter to populate the envelope of the model. The slopes of the straight lines fitted to these data should differ in magnitude by the ratio of the particle masses, since total energy conservation requires the energy lost by the heavy particles to be taken up by the light. In practice, this symmetry is imperfect because of the large measurement uncertainties. Henceforth, I report only the slopes, multiplied by  $\mu$ , and their statistical uncertainties.

Were two-body encounters the only source of relaxation, energy exchange between particles of the different mass species would not be partly masked by short term oscillations. That short-term changes in the right panel are larger than the gradual diverging trend is evidence that relaxation, measured in the left-hand panel, is being driven mostly by the collisionless (collective) oscillations of the model discussed above that are unaffected by particle masses.

#### 4.3. Measures of relaxation rate

Figure 4 summarizes the relaxation measurements from all 27 simulations. The three rows show the three different mass models; within each panel there are three different numbers of particles, and for each case, the evolution was computed by three separate force determination methods. The measured rates from the heavy particles are shown in red, while those from the light particles are marked in green, and the uncertainties in the slopes are indicated by the error bars, that are often too short to be visible. The different force determination methods used are distinguished by the different symbol types as indicated in the figure caption, and offset horizontally from each other for clarity even though the particle numbers are the same. These conventions are the same in the left and right panels.

The left panels show the energy diffusion rate, defined as

$$\langle E_i(0) \rangle^{-2} \frac{d}{dt} \langle [E_i(0) - E_i(t)]^2 \rangle \quad (4)$$

in units of  $t_0^{-1}$ . The adopted values for  $\langle E_i(0) \rangle$ , which are  $-0.3$ ,  $-0.45$ ,  $-0.9$  for the Hernquist, Plummer, and uniform sphere respectively, are the same for all nine simulations with each model. The straight dotted line has slope  $-0.5$  while the dashed line shows the function  $A \ln N/N$  with  $A = 0.1$ ; these lines are not fits to the data and are for comparison only. The right panels show  $N d\langle E_i(t) \rangle / dt$ , the factor  $N$  for each sub-population is included for clarity – in reality, the slopes roughly decrease as  $1/N$ .

There are many conclusions to be drawn from these data.

First, the differences between the energy diffusion rates (left panels) for the heavy (red) and light (green) particles within one simulation are generally small. This is a further indication of the dominance of collective modes, which cause deflections that are independent of particle mass, in driving this measure of relaxation.

Second, the energy diffusion rate declines roughly as  $N^{-1/2}$  in the uniform sphere, whereas in the inhomogeneous models it declines more or less with the expected

$\ln N/N$  dependence for collisional relaxation. If 2-body effects were dominant in all cases, the variation with  $N$  should be the same in all three mass models. The absolute values cannot be compared with the predicted 2-body relaxation rate (Binney & Tremaine 2008), because the energy diffusion rate is a different measure of relaxation.

Third, the rates of energy exchange shown in the right hand panels generally have opposite signs, and vary roughly as  $N^{-1}$ , since they are approximately constant when multiplied by  $N$ . The values from the highest  $N$  experiments are quite uncertain, because the decreasing variation in the mean as  $N$  rises is masked by short-term changes (see the right panel of Fig. 3) – *i.e.* the trends decrease into the noise. This is particularly problematic for the uniform sphere (bottom right panel), where the potential changes associated with pulsations of the model dominate over the energy exchange rate at the highest  $N$ , making an accurate measurement over the time interval simulated impossible.

Fourth, the different methods used to compute the gravitational field yield broadly similar behavior in all three mass models, and the variation of the rates with  $N$  in both the left and right panels is similar for each method in each of the different models.

Fifth, the energy diffusion rate (left panels) is consistently lower, but by a factor  $< 3$ , for the SFP method (diamonds) than for the tree code (crosses) and the spherical grid (circles) in the Hernquist and Plummer models. Hernquist & Ostriker (1992) also reported a slightly lower energy diffusion rate when they used a field method, although it was unclear whether the more rapid diffusion in their tree code, for example, resulted mainly from the mild disequilibrium of their initial model caused by gravity softening. However, the mass segregation rate (right panels), which is a cleaner measure of 2-body relaxation, is no less for SFP than for the other methods.

The reason for the slightly lower diffusion rate in the field method is unclear. Both the SFP and S3D methods employ an expansion in surface harmonics up to  $l_{\max} = 8$  to capture any angular variations, and the principal difference between them is radial resolution: the SFP method employs 11 radial functions ( $0 \leq n \leq 10$ ), while the S3D uses a grid of  $\sim 100$  radial shells. It therefore seemed that the marginally higher energy diffusion rate when the S3D grid was used was because that grid could support more oscillatory modes. However, increasing the number of radial functions used in the SFP method to 51, in order to enable the field method also to support more collective modes, led to little change in either measure of the relaxation rate, confounding this theory!

Sixth, relaxation in the uniform sphere probably is completely dominated by the oscillatory modes excited by the shot noise in the particle distribution. The initial amplitudes of the modes should scale as  $N^{-1/2}$ , and the decline in relaxation rate with approximately this dependence in the uniform sphere is a direct indication of their dominance in this case. Collective modes are present in all models, but the different  $N$ -dependence in the inhomogeneous models probably results from resonant damping of the modes.

Seventh, short-range gravity softening appears to have little effect on the relaxation rate. There is no explicit softening in SFP, and the only smoothing on the spherical grid

is linear interpolation in radius. Force softening is explicit in the tree code and implicit in the C3D grid, where forces are slightly sharper  $\epsilon_{\text{eff}} = 0.036a$  while  $\epsilon = 0.05a$  for the BHT code for the uniform sphere. Yet the relaxation rates scarcely differ between the various codes. This emphasizes the dominance of distant encounters, enhanced by collective oscillations, in driving relaxation and that softening's only value is to avoid large accelerations during close encounters between particles, which would require short time steps to integrate the motions accurately.

## 5. CONCLUSIONS

The main result here confirms that previously found by Hernquist & Barnes (1990) and by Hernquist & Ostriker (1992) that the rate of relaxation in  $N$ -body simulations that aspire to be collisionless is very largely independent of the method used to compute the gravitational field. This is especially true when the relaxation rate is assayed as the rate of energy exchange between particles of different masses – see the right hand panels of Fig. 4. This result is physically reasonable, since relaxation is dominated by distant encounters and any method that correctly yields the field from distant particles must faithfully include their stochastic contributions. Thus the calculation by Weinberg & Katz (2007a,b) that the relaxation time scale is orders of magnitude longer in field methods must be in error.

The rate of relaxation, defined more generally as the rate of energy diffusion, arises from at least two distinguishable sources: the deflections caused by 2-body encounters, and the effects of collective oscillations of the system. The rate of energy exchange between particles of differing masses is a more direct measure of 2-body relaxation, but this could not be measured very precisely because collective modes were so dominant unless the number of particles is comparatively modest.

The different  $N$ -dependence in the uniform sphere (bottom left panel of Fig. 4) is clear evidence that collective modes dominate the relaxation in this case. This model differs from the other two by having a harmonic potential throughout in which the orbit frequencies of all particles are the same; this difference permits undamped collective oscillations, whereas collective modes are damped in the other cases.

The slightly lower energy diffusion rates that result from use of the field method (diamonds in top left and middle left panels of Fig. 4) is bought at a high price. The leading term in the basis used for both cases was a perfect match to the equilibrium model, and the same basis would be less suited were the density to evolve, or were it used for any other model, requiring more terms to yield the correct total potential. Thus field methods lack the versatility to follow arbitrary changes to the distribution of mass within a model unless the expansion is taken to higher order, and their slightly better relaxation rate can be achieved in any of the more general methods simply by employing a few times more particles. A real advantage of field methods, featured by Weinberg & Katz (2007a,b), is that they offer an elegant comparison of simulations with perturbation theory when computing first order changes to an equilibrium model that could be unstable or externally perturbed.

The energy diffusion time scale, the inverse of the rate defined in eq. (4) and plotted in Fig. 4, is  $\gtrsim 10^5$  dynamical times for only  $N = 4 \times 10^5$  particles in the inhomogeneous models. Thus simulations of inhomogeneous 3D models that employ any valid code require larger numbers of particles, but not by a large factor, if relaxation times defined by this measure are to be safely longer than the ages of the galaxies being simulated.

## ACKNOWLEDGMENTS

The author wishes to thank Tad Pryor and Joel Berrier for helpful conversations. This work was supported by NSF grant AST/1108977.

## REFERENCES

- Barnes, J. & Hut, P. 1986, *Nature*, **324**, 446  
 Binney, J. & Tremaine, S. 2008, *Galactic Dynamics* (2nd ed.; Princeton: Princeton University Press)  
 Clutton-Brock, M. 1972, *Ap. Sp. Sci.*, **17**, 292  
 Hernquist, L. 1990, *ApJ*, **356**, 359  
 Hernquist, L. & Barnes, J. E. 1990, *ApJ*, **349**, 562  
 Hernquist, L. & Ostriker, J. P. 1992, *ApJ*, **386**, 375  
 Hockney, R. W. & Eastwood, J. W. 1981, *Computer Simulation Using Particles*, New York: McGraw Hill  
 James, R. A. 1977, *J. Comp. Phys.*, **25**, 71  
 McGlynn, T. A. 1984, *ApJ*, **281**, 13  
 Monaghan, J. J. 1992, *ARAA*, **30**, 543  
 Plummer, H. C. 1911, *MNRAS*, **71**, 460  
 Polyachenko, V. L. & Shukhman, I. G. 1979, *Astron. Zh.* **56**, 724; English translation: 1981, *Soviet Ast.*, **25**, 533  
 Rostoker, N. & Rosenbluth, M. N. 1960, *Phys. Fluids*, **3**, 1  
 Sellwood, J. A. 2003, *ApJ*, **587**, 638  
 Sellwood, J. A. 2013, *ApJL*, **769**, L24  
 Sellwood, J. A. 2014, arXiv:1406.6606 (on-line manual: <http://www.physics.rutgers.edu/~sellwood/manual.pdf>)  
 Sellwood, J. A. & Merritt, D. 1994, *ApJ*, **425**, 530  
 Springel, V. 2005, *MNRAS*, **364**, 1105  
 Weinberg, M. D. 1998, *MNRAS*, **297**, 101  
 Weinberg, M. D. & Katz, N. 2007a, *MNRAS*, **375**, 425  
 Weinberg, M. D. & Katz, N. 2007b, *MNRAS*, **375**, 460